PCCP

Accepted Manuscript

ROYAL SOCIETY OF CHEMISTRY

www.rsc.org/pccp

Journal Name

ARTICLE TYPE

Cite this: DOI: 10.1039/xxxxxxxxxx

Photoelectron diffraction in methane probed via vibrationally resolved inner-valence photoionization cross section ratios

Saikat Nandi,[a] Etienne Plésiat,[b] Minna Patanen,[a‡] Catalin Miron,[a,d] John D Bozek,[a] Fernando Martín,[b,e,f] Daniele Toffoli,[c] and Piero Decleva*[c]

Received Date
Accepted Date

DOI: 10.1039/xxxxxxxxxx

www.rsc.org/journalname

Vibrationally resolved photoionization of the $2a_1$ orbital in methane has been studied both experimentally and theoretically, over a wide range of photon energies ($40-475$ eV). A vibrational progression associated to the symmetric stretch mode of the $2a_1^{-1}$ single-hole state was observed in the experimental photoelectron spectra. Individual vibrational sub-states of the spectra were found to be best modeled by asymmetric line-shapes with linewidths gradually increasing with vibrational quantum number. This indicates the occurrence of a pre-dissociation process for the involved ionic state, discussed here in detail. Finally, diffraction patterns were observed in the vibrational branching ratios for the first three vibrational sub-states ("v-ratios") of the experimental photoelectron spectra. They are found to be in excellent qualitative agreement with those obtained from ab-initio models. Compared with previous studies of the $1a_1^{-1}$ core-shell photoionization of methane, the period of oscillation of the v-ratios is found to be very different and the phases of opposite sign. This suggests a strong interplay between the electron diffraction and interference effects inside the molecular potential.

1 Introduction

Interference effects in molecular photoionization[1–15] as well as in ionization by electron impact[16,17] or heavy ion scattering[18–20] have been extensively studied in recent years. Two distinct types of interference processes have been observed to play an important role in molecular photoionization. One originates from coherent emission from equivalent centers in a molecule and the other from the interference of a wave scattered from neighboring centers with the primary wave. The second process is referred to as photoelectron diffraction. In the case of ionization from delocalized molecular orbitals, however, both often coexist and the distinction somewhat becomes blurred. Interference and diffraction phenomena lie at the foundation of quantum mechanics, the former being the analogous of the celebrated Young's double-slit interference[21–23], the second traced back to the first confirmation of the wave-particle duality observed by C. J. Davisson and L. H. Germer in 1927[24]. The signature of diffraction processes in photoemission from free molecules has been realized only recently, although it underlies the well-known extended X-ray absorption fine structure (EXAFS) oscillations in core X-ray absorption, and becomes an analogous method for structural determination. Although photoemission experiments are more technically demanding than total absorption methods, they afford a broader range of experimental conditions and choice of observables. Foremost is the possibility to select a specific ionization channel, from deep core-shells to outer valence-shells, allowing the choice of most suitable and well-resolved photoelectron bands. Furthermore, partial photoelectron cross sections can be obtained for individual chemically inequivalent atoms in a molecule, which will not be uniquely identifiable in a total cross section measurement. Many observables can be followed: partial cross sections, vibrational branching ratios, asymmetry[25] and non-dipole parameters[26], up to full molecular frame photoelectron angular distributions (MFPADs)[27]. Ion state resolved cross section ratios are independent of the underlying cross sections of other available ionization processes, obviating the problematic baseline due to the very

[a] Synchrotron SOLEIL, L'Orme des Merisiers, Saint-Aubin, BP 48, 91192 Gif-sur-Yvette Cedex, France. E-mail: saikat.nandi@synchrotron-soleil.fr
[b] Departamento de Química, Módulo 13, Universidad Autónoma de Madrid, Cantoblanco 28049, Madrid, Spain.
[c] Dipartimento di Scienze Chimiche e Farmaceutiche, Universita di Trieste, Via L. Giorgieri 1, 34127 Trieste, Italy. E-mail: decleva@units.it
[d] Extreme Light Infrastructure - Nuclear Physics (ELI-NP), 'Horia Hulubei' National Institute for Physics and Nuclear Engineering, 30 Reactorului Street, RO-077125 Măgurele, Jud. Ilfov, Romania.
[e] Instituto Madrileño de Estudios Avanzados en Nanociencia (IMDEA Nano), Cantoblanco, 28049 Madrid, Spain.
[f] Condensed Matter Physics Institute (IFIMAC), Universidad Autónoma de Madrid, 28049 Madrid, Spain.
‡ Present address: Nano and Molecular Systems, Faculty of Science, BOX 3000, 90041 University of Oulu, Finland.

rapid decrease of the cross sections with increasing photon energy, which cannot be avoided in total yield EXAFS data. Finally, beyond geometrical information, photoemission observables are deeply connected to the electronic structure of the target, which is imprinted in the dynamical behavior of the observables.

To extract useful structural information from the photoelectron diffraction patterns a theoretical modeling framework is absolutely necessary. Unfortunately, no accurate simple analytical model is presently available, and one has to resort to fully quantum mechanical calculations to retrieve the basic information. Efficient and reasonably accurate theoretical approaches are available for this purpose, although their limit of validity still remains to be evaluated. Clearly, further development of reasonably simple analytical models[11,13,28] would boost the applicability of the technique as a structural tool. At this stage, however, a basic understanding is still to be gained from exploring the behavior of the diffraction patterns in different simple controlled situations to demonstrate the applicability of the technique and the currently available computational models.

It has recently been demonstrated that both interference and diffraction effects appear in vibrational branching ratios (v-ratios), obtained from the ratios of the intensities of individual vibrational components (sub-states) within a single electronic final state[8,11,28]. These studies show significant variations of the v-ratios around those predicted at the Frank-Condon (FC) level. Although requiring vibrational resolution, a specific advantage of the v-ratios is the possibility of studying interference and diffraction effects in a single ionization channel, and moreover to provide information on the geometry of both the initial and final electronic states[12]. Such a structural probe can be very sensitive and can reveal even the very weak diffraction associated with light hydrogen atoms as was shown for core shell ionization of CH_4[11]. In the present study we have focused on v-ratios from inner-valence $2a_1$ ionization of methane. The ground-state electronic configuration of methane is $(1a_1)^2(2a_1)^2(1t_2)^6$. Ionization from the outer valence orbital $(1t_2)$ leads to a triply degenerate state $^2T_2$, which is split into different components, each with different energies in the Franck-Condon region, due to the Jahn-Teller interaction[29]. In contrast, ionization from the $2a_1$ orbital shows an extended, well-resolved vibrational progression, which appears ideally suited for such study. Photoionization of core level electrons from the $1a_1$ orbital in methane have been reported in several studies[30–33]. On the other hand studies involving photoionization of inner-valence, $2a_1$, orbital in methane are relatively scarce[34].

The present work has been carried out to extend v-ratio measurements to the inner-valence region of the CH_4 molecule by means of photoelectron spectroscopy using monochromatic X-rays at high energy resolution. Beyond exploring the general feasibility of diffraction studies of v-ratios in the valence-shell, the further aim is to investigate the sensitivity of v-ratios to the ionization channel, i.e. to the ionized orbital, by comparing the present results with core, $1a_1$ (C $1s$), ionization previously reported[11]. In the previous $1a_1$ case, only the totally symmetric motion is excited (neglecting recoil effects[11,12,35]) by C $1s$ photoionization. The oscillation period of the diffraction pattern is then determined by the distance between the emitter and the scattering centers, while the magnitude of the v-ratios remains sensitive to the change of equilibrium geometry between the neutral and ionic states. Consequently, the oscillation periods in both $1a_1$ and $2a_1$ ionization v-ratio profiles are expected to be similar, with different v-ratio baselines due to the much larger change of the C-H distance $\left(\Delta R = +0.106 \text{ Å, present results}\right)$ in the $2a_1^{-1}$ ion compared to the minor shortening $\left(\Delta R = -0.048 \text{ Å}\right)$ in the $1a_1^{-1}$ cation[36]. This is immediately apparent from the $2a_1$ photoelectron spectra exhibiting an extended vibrational structure with reduced vibrational frequency: 2160 cm^{-1} (present results) against 3352 cm^{-1} in the $1a_1^{-1}$ cation[36].

To verify the extent to which these expectations are borne out, and our general understanding of diffraction effects in v-ratios, we have undertaken a joint experimental and theoretical study of the $2a_1$ photoemission from CH_4. A previous analysis[34] of the vibrational photoelectron spectrum serves as initial guide to this study.

The following manuscript has been divided into these sections: an overview of the experimental results and data analysis, details of the theoretical model, results and discussions, and finally, conclusions.

2 Experimental setup

The experiments were carried out at the PLÉIADES beamline[37] of Synchrotron SOLEIL, the French national synchrotron radiation facility in Saint Aubin (91). The details of the beamline can be found elsewhere[38], so only a brief overview of the main components is mentioned here. An Apple II-type permanent magnet undulator with 80 mm period was used to produce the linearly polarized synchrotron radiation. It was then monochromatized using a variable groove depth, variable line spacing plane grating. Two different gratings, one with 600 lines/mm (high-flux) and another with 2400 lines/mm (high-resolution) were used in this study. The methane inner-valence photoelectron spectra (PES) were recorded at the so-called "magic" angle of 54.7° with respect to the light polarization vector using a wide-angle lens VG Scienta R4000 spectrometer. This ensured the photoionization cross sections to be free from the photoelectron emission anisotropy over the entire range of incident photon energies.

High purity (99.995%) methane from Air Liquide was used as target inside a differentially pumped gas cell. The gas cell was equipped with five electrodes to compensate the plasma potentials present in the interaction region due to an ion density gradient created along the synchrotron radiation beam. Throughout the entire experiment, the pressure was kept below 1×10^{-5} mbar in the spectrometer chamber to avoid detector saturation at low photon energies, the pressure inside the gas cell being typically two orders of magnitude higher than that in the main chamber.

The pass energy for the spectrometer was fixed at either 20 or 50 eV. The curved entrance slit of the analyzer was kept at 0.3 mm throughout the experiment. The photon bandwidth was adjusted by changing the width of the exit slit of the monochromator. It was varied from $7 - 200$ μm during the experiment to obtain the desired photon energy resolution along with a suitable photon

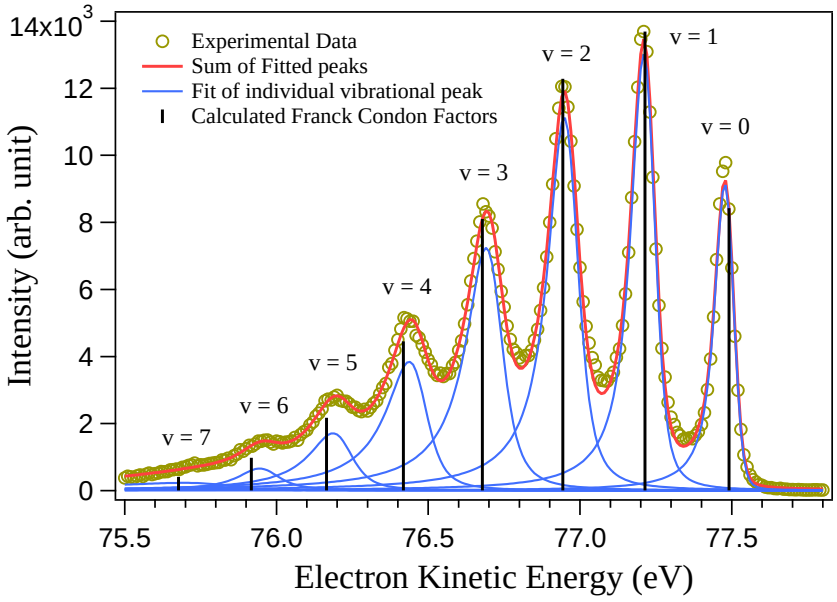

Fig. 1 Vibrationally resolved, inner-valence $(2a_1)$ photoelectron spectrum of CH_4, measured with a photon energy of $100\,(\pm 0.1)$ eV. The vibrational progression corresponds to the symmetric stretching mode in the CH_4^+ ion with a $2a_1$ hole. The assignment to the vibrational sub-levels closely follows that found by Göthe *et al*[34]. The experimental spectrum was fitted using PCI line shapes as described in the text to conveniently account for the observed asymmetry which is attributed to predissociation of the cation. The Franck-Condon (FC) factors were calculated using the diabatic CASSCF/NEVPT2 potentials. The intensities for the FC factors are normalized to the experimental intensity of the $v = 1$ sub-level.

flux. As expected, the photon energy resolution was highest at the lowest photon energy. At higher energies, where the photoionization cross section and the photon flux both decrease, the flux was increased by opening the exit slit, thereby degrading the photon energy resolution. Overall, the photon energy resolution varied between $2-60$ meV in the range of excitation energies used in the experiment. The translational Doppler broadening for CH_4 molecules at room temperature was estimated to be within $12-66$ meV, while the rotational Doppler broadening is expected to be on the same range[39] depending on the electron kinetic energy and the ionized molecular orbital[40]. Combining all three contributions, the total experimental broadening was estimated to be $13-85$ meV, throughout the experiment (rotational Doppler broadening not included). Additionally, the well-known Helium $1s^{-1}$ photoelectron line was measured at a few photon energies to verify the experimental resolution.

3 Data analysis

A typical photoelectron spectrum of the inner-valence ($2a_1$ state) photoionization in methane measured at $100\,(\pm 0.1)$ eV is shown in Figure 1. This spectrum and others measured at other photon energies were fitted with the least squares curve fitting macro package SPANCF[32,41,42] for Igor Pro. Post collisional interaction (PCI) distorted asymmetric line shapes were found to provide the best fit to the measured spectra. The spectra were analyzed by keeping the Lorentzian widths for each vibrational line fixed for all spectra. The Lorentzian widths for $v = 0$, 1, and 2 are estimated to be 35, 65 and 95 meV, respectively, for all the spectra. Gaussian widths were allowed to vary with photon energy to accommodate the changing resolution but the width for each vibrational line was fixed to that of the lowest $(v = 0)$ vibrational level for a given photon energy. The asymmetry for each vibrational level was fixed at that obtained for the lowest photon energy. Finally the energy spacing between excited vibrational levels $(v > 0)$ and the lowest $(v = 0)$ one was fixed for all spectra. The spacing between the first two lines, 0.2677 eV $(2160\ \mathrm{cm}^{-1})$, compares well with the previously reported value of 0.269 eV[34].

The observed asymmetry of the vibrational lines in the $2a_1$ photoelectron spectra of CH_4 is not attributed to the PCI affect which occurs in core-shell ionization spectra at photon energies where the photoelectron is less energetic than the Auger electron. As Auger decay does not occur here, a different mechanism must cause the asymmetry. Asymmetry and irregularity of the vibrational structure was already noted in previous work[34] and attributed to pre-dissociation caused by the crossing of the potential energy curves of states lying higher at the equilibrium geometry (satellite states), becoming lower in energy as the bonds are symmetrically stretched. Thus, the coupling between a bound and a repulsive state can be considered as the onset of pre-dissociation for the molecular ionic state. In addition to significantly broadening the spectral lines, the pre-dissociation can also account for the observed asymmetry. According to previous electron impact ionization measurements[43] carried out above the ionization threshold of the $2a_1$ orbital in CH_4, the existence of H^+ ions in the corresponding decay channels was also attributed to the possible opening of a pre-dissociation channel in the excited CH_4^+ ions.

Figure 1 clearly shows that the widths of the spectral lines increase continuously with increasing vibrational quantum number. In fact, for higher vibrational sublevels, the overlap between neighboring levels becomes significant, indicating the strong influence of the pre-dissociation in the molecular ion. Consequently, only the first three, i.e., $v = 0$, 1 and 2, levels are suf-

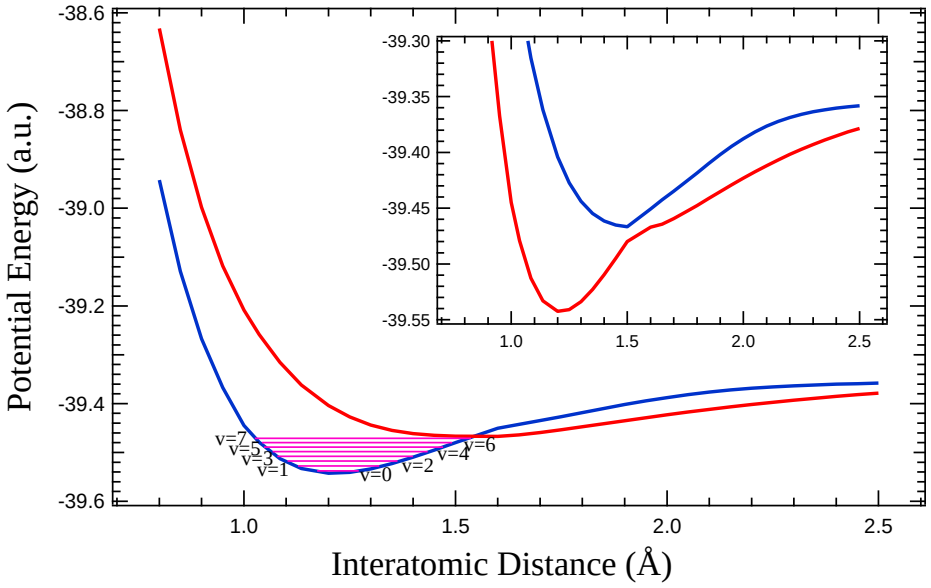

Fig. 2 Adiabatic (inset) and Diabatic potential energy curves for the symmetric stretching mode in the CH_4^+ ion with $2a_1^{-1}$ hole state calculated as a function of interatomic distance. The 'avoided crossing' between the 1^{st} and 2^{nd} ionic state is clearly visible. The horizontal lines show the calculated energies of different vibrational sub-levels corresponding to the diabatic potential energy curves. Note the close proximity of the higher vibrational sub-levels to the satellite state.

ficiently resolved to accurately study the effect of photoelectron diffraction in v-ratios. The area under each peak was used to describe the relative intensities rather than the peak height. Poisson counting statistics was assumed for which the standard error is the square root of the number of counts. Finally, uncertainties of the v-ratios for the corresponding vibrational sub-levels were obtained as the square root of the sum of the squares of the two uncertainties relative to the area under each peak.

4 Theoretical models

The theoretical model used in our research follows closely the one earlier employed for the study of $1a_1$ photoionization in methane[11]. It has been described in detail previously[44,45] and has been shown to produce excellent agreement with the experiments; here we limit ourselves to summarize only the main steps. The method provides a solution of the scattering problem in a Density Functional Theory (DFT) framework and utilizes a discretization of both bound and continuum wave-functions in a multi-center basis of B-spline functions $B_i(r)$ multiplied by real spherical harmonics $Y_{lm}(\theta,\phi)$,

$$\chi_{ilm} = \frac{1}{r} B_i(r) Y_{lm}(\theta,\phi).$$

The bound states are calculated by a conventional generalized diagonalization of the Kohn-Sham Hamiltonian matrix while the continuum states are obtained from a least squares approach within the static exchange approximation.

The SCF initial electronic density of the ground state is first obtained by a standard Linear Combination of the Atomic Orbitals (LCAO) approach with the ADF program[46]. A transition state density (half an electron removed from the $2a_1$ orbital) was employed. The pure LDA exchange-correlation potential is employed, with a DZP basis set for C and H atoms taken from the optimized database included in the ADF package. From the transition state density, a fixed Kohn-Sham Hamiltonian is obtained and it is further diagonalized in the B-spline basis both for the bound and the continuum states (static-exchange DFT approach). The B-spline basis set comprises a long range expansion around a common origin (one center expansion), with large angular momenta, to describe the continuum wave-functions up to the asymptotic coulomb region, where they are fitted to analytical solutions, and a set of additional functions centered on the various nuclei, in the spirit of the LCAO approach, which takes care of the Coulomb singularities at the nuclei, and ensure fast convergence of the expansion. In the present calculation, 400 splines of order 10 have been employed over an interval up to $R_{max} = 25$ atomic units (a.u.) for the one center expansion and maximum angular momentum up to $L_{max} = 13$. For the expansion around the hydrogen atoms $L_{max} = 1$ was employed, and $R_{max} = 0.5$ a.u. for the radial expansion. Those choices ensured complete convergence of the calculated cross sections and branching ratios.

Potential energy curves (PECs) of the symmetric stretching mode for the ground state and the $2a_1^{-1}$ ion were computed at the CASSCF/NEVPT2 level[47,48] with the program MOLPRO[49], employing an active space comprising the 4 bonding and 4 antibonding orbitals and a cc-PVTZ basis. The energy was computed for 34 points spanning the interval $(0.800 - 2.500)$ Å for the C-H distance. As discussed below in more detail, avoided crossings became apparent in the $2a_1^{-1}$ state (see Figure 2), and we diabatized the resulting potential energy curves by switching values between the two states at the crossing point $\left(R = 1.6\,\text{Å}\right)$. The computed equilibrium distance R_e

(1.1068 Å for the ground state and 1.2126 Å for the ionic state) and the first vibrational frequency already reported are in good agreement with the experimental data available. Indeed, the computed elongation in the $2a_1^{-1}$ ion is close to that obtained by Meyer[50], but significantly smaller than the value of 0.185 Å obtained by Göthe *et al.*[34] using FC analysis of the experimental spectrum, which appears quite overestimated. With the resulting PECs, accurate vibrational wave-functions were obtained by solving the vibrational Schrödinger equation in a basis of 1000 B-splines within a box of 5 a.u.

Electronic dipole matrix elements were computed for 200 photoelectron energies and 64 inter-nuclear distances relative to the symmetric stretching coordinate. Finally, vibrationally resolved dipole transition matrix elements were evaluated by integrating the electronic dipole moments, interpolated for the correct energy, between initial and final vibrational wave-functions.

5 Results and discussions

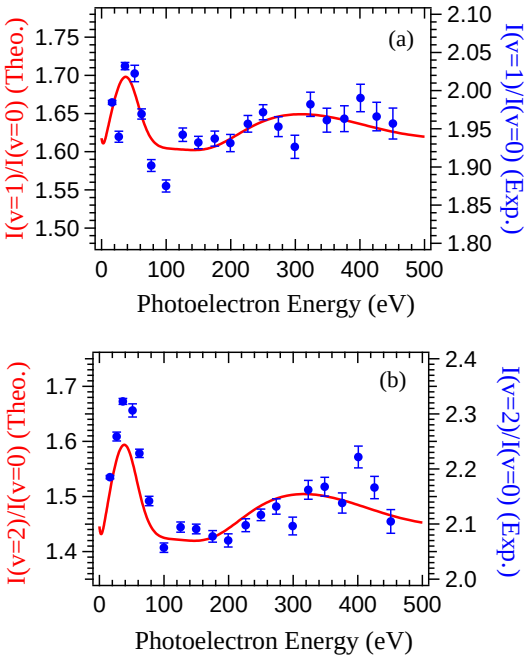

Fig. 3 Vibrational branching ratios for photoionization of $2a_1$ orbital leading to excitation of the symmetric stretching mode in CH_4^+ ion as a function of the photoelectron energy [Photon energy - Vertical binding energy of $2a_1$ orbital (23 eV)[34]]. In both panels the solid line corresponds to the density functional theory (DFT) theoretical results. Note the difference in scale for experimental and theoretical results, in both the panels.

From the typical spectrum given in Figure 1, both the quality of the fitting of experimental data and the reproduction of energies and intensities of the various vibrational sub-states is apparent. Despite a good general agreement, some deficiencies are clearly visible. As already mentioned, the asymmetry and irregularity of the vibrational peaks are a signature of vibronic coupling with dissociative states that cross the diabatic curve relative to symmetric C-H stretching in the $2a_1^{-1}$ cation, noticed and discussed previously[34]. The ground state of the CH_4^+ ion with a vacancy in the $2a_1$ orbital is actually a few eV above the threshold for dissociation into CH_3 and H^+. Apart from the nonphysical dissociation $C^+ + 4H$ along the symmetric stretching, a number of satellite states with leading configurations: $(1a_1)^2(2a_1)^2(1t_2)^4(2t_2)$ and $(1a_1)^2(2a_1)^2(1t_2)^4(3a_1)$ around 29.2 and 32.1 eV binding energy, respectively, have been identified[34,51]. At the equilibrium geometry of the neutral molecule, these states lie well above the $2a_1^{-1}$ state, however the satellite states are dissociative and the potential energy curves cross at geometries with larger C-H bond distances. A clear sign of this crossing was observed when computing the potential energy curves for the $^2A_1$ states of the cation at the CASSCF/NEVPT2 level. The results obtained are reported in Figure 2, where the avoided crossing between the first and the second ionic state is clearly visible. At the avoided crossing the Born-Oppenheimer approximation breaks down. This indicates a strong vibronic coupling between the electronic and nuclear coordinates. In this situation, the system initially in the first excited state can have a non-zero probability for leaking into the dissociative satellite state.

Now instead of considering the adiabatic surfaces, one can construct non-adiabatic surfaces that are allowed to cross each other (see Figure 2), thus leading to a conical intersection as a result of the corresponding electronic states of same symmetry. We manually diabatized the potential energy curves for the $2a_1^{-1}$ configuration by smoothly joining them around the avoided crossing. The increasing disagreement of calculated energies and Franck-Condon (FC) factors with increasing vibrational number is however clearly seen in Figure 1. Despite the amplitude of the lowest cationic vibrational states lying in the Franck-Condon region close to the bottom of the curve, their pre-dissociative nature makes both the experimental and computed v-ratios quite sensitive to the details of the fitting and the potential energy curves employed, which is probably the main cause of the discrepancies between the experimental and computed values for the $v = 1/v = 0$ and $v = 2/v = 0$ v-ratios.

Figure 3 shows the experimental and theoretical v-ratios as a function of photoelectron energy. The theoretical results are in very good qualitative agreement with the experimental values. The expected oscillations are clearly revealed, and the oscillation period appears to be correctly reproduced. One should note that the measurement of v-ratios is free from any normalization artifacts that might affect the overall trends observed in absolute cross sections over the photon energy range. In both cases, for electron kinetic energies below 150 eV, the statistical errors on the v-ratios are less than 1%. Beyond that, the uncertainty increases steadily and, at the highest energies, it is as large as 2%. The reason for this may be found in the fact that at higher photon energies the cross sections decrease sharply, thereby making collection time for statistically significant number of counts very long. At the highest photon energy it was around 90 minutes, compared to that of $5-8$ minutes at lower photon energies, to collect statistically significant number of counts for the intense-most $v = 1$ vibrational sub-state.

While the pronounced oscillation in the v-ratios and the general behavior of the oscillation in the experimental data are qualitatively very well reproduced by the theoretical calculations,

one should note the different scale for the experimental and theoretical v-ratios. Theory underestimates the experimental $v = 1/v = 0$ ratios by 20%; in the case of the $v = 2/v = 0$ ratios the underestimation is close to 40%. In addition, the amplitude of the oscillation in the experimental data is underestimated by approximately 10% in the theoretical calculations. Since the absolute values of the v-ratios, i.e. the baseline, are mainly determined by the FC factors, which are extremely sensitive to the change in the C-H distance upon ionization, we attribute this disagreement mostly to a slightly inaccurate value of our ab-initio computed surfaces as indicated by the large discrepancy between the bond elongation presently computed here compared to that reported previously[34].

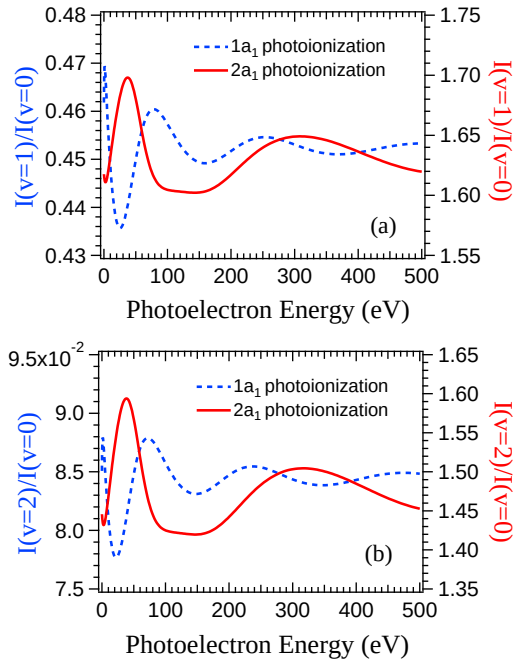

Fig. 4 Theoretical vibrational branching ratios [$I(v = 1)/I(v = 0)$ (panel a) and $I(v = 2)/I(v = 0)$ (panel b)] compared between $1a_1$ [11,12] (dashed line) and $2a_1$ (solid line) hole states of methane. The phases corresponding to the different hole states are of opposite sign for both the v-ratios. Also, the period of oscillation is longer in the case of $2a_1^{-1}$. In both the panels, the scale on the left (right) correspond to the $1a_1$ ($2a_1$) hole state. Note the difference in scale for the two hole states, in both the panels.

The peak at relatively low photoelectron energy, about 40 eV, is probably the signature of a shape resonance, although none has been reported in the total cross section or angular distributions of CH_4 photoelectrons. A similar peak, although reversed, is also apparent in the v-ratios for $1a_1$ photoionization[11,52] at a slightly lower energy (see Figure 4 for comparison). It appears then that v-ratios are extremely sensitive even to rather low intensity shape resonances. This is due to the fact that as the resonance appears at slightly different photon energies in two vibrational channels, it is much enhanced in the v-ratio, as was observed in CF_4[14]. A small structure present in the core-shell photoionization spectrum[53], and attributed either to a shape resonance or the presence of doubly excited states, is too close to threshold to match the present results. Moreover, the presence of the same features both in $1a_1$ and $2a_1$ ionization rules out the effect of doubly excited states. The experimental v-ratio profiles exhibit a sharper peak profile than the calculated one, something that is suggested also in the $1a_1$ case. In the absence of a very fine scan of the low energy region, it is difficult to ascertain the extent of the disagreement, which could be due to inaccuracies either of the potential energy curves, or of the electronic wavefunctions, expected to be less accurate at lower kinetic energies. The oscillatory behavior is expected to be smoother at higher energy, and indeed the experimental points match quite well the calculated profiles, especially for the $v = 2/v = 0$ ratio (see Figure 3(b)), despite some scattering of the individual values.

The oscillatory structure can be associated to electron diffraction as the outgoing electron wave scatters from the surrounding H atoms. In our LCAO representation of molecular orbitals (MOs), one can see that the $2a_1$ orbital has contributions not only from the C $2s$ atomic orbital (AO), but also from the H $1s$ orbitals. Due to the extended nature of this MO, the cross-section oscillation carries also contributions from multi-center interference effects. Kushawaha *et al.* studied inner valence photoionization cross sections of simple hydrocarbons with two C atoms, observing an oscillatory structure in the ratio of the cross sections of gerade (g) and ungerade (u) symmetry states[9]. In their case, the two carbons can be thought to be like two slits in a Young's double-slit experiment, and the oscillatory behavior was explained as originating from the corresponding interference effects. When they compared the calculated g/u cross section ratios of different molecular orbitals, they noticed that in the "pure" double-slit case, namely C $1s$ derived MOs, the amplitude of the oscillations are varying regularly around unity whereas asymmetric oscillations were found for the C $2s$ derived MOs. The irregularity was interpreted to bear information on the AO combination of the C $2s$ derived MOs, as the H $1s$ orbitals contribute significantly to these orbitals, thus breaking the pure double-slit picture.

The theoretical v-ratios for inner-valence photoionization are compared with those calculated for core-shell photoionization of methane (see Figure 4). For both the single-hole states, the symmetric stretching vibrational mode is considered. Surprisingly, the expected similarity in oscillation period for $1a_1$ and $2a_1$ ionization processes is not borne out. Not only is the phase of the oscillations in v-ratios for $1a_1$ and $2a_1$ photoionization found to be opposite, but also the period of the oscillations is larger and asymmetric in the case of $2a_1$ compared to $1a_1$. The final continuum states are very similar for photoionization from both the inner-shell and inner-valence orbitals. The initial state is, however, quite different in the two cases, both in shape and in spatial extension (see Figure 5).

In contrast to the previous study by Kushawaha *et al*[9], in this case the $1a_1$ orbital is centered on the carbon nucleus, effectively having only a C $1s$ character, and thus, oscillations originate purely from scattering from surrounding hydrogen atoms. The $2a_1$ orbital includes significant overlap between the carbon $2s$ atomic orbital as well as the neighboring $1s$ orbitals of the four hydrogen atoms. The Mulliken population of the DFT LCAO wavefunction gives very close to 50% for both the carbon $2s$

and the hydrogen $1s$ contributions for the $2a_1$ orbital. The difference in phase and period thus highlights effects resulting from electron delocalization over the whole molecule. It is interesting to speculate on the reason of larger oscillation period in the $2a_1$ ionization compared to $1a_1$. The former orbital is more extended, and closer to hydrogen atoms. Because of the inverse relationship between bond distance and diffraction oscillation period, this could lead to the observed pattern.

Alternatively, for photoemission from the $1a_1$ orbital, the path-length difference responsible for the diffraction pattern is approximately twice the C-H bond length; the ionized electron wave (originating from a localized core-hole) gets partially scattered by the surrounding H atoms, and subsequently interfere with the initial wave resulting in the oscillatory structure. For photoemission from the $2a_1$ orbital, one can consider the oscillatory structure as a result of the coherent emission from an orbital delocalized over the entire molecule; the C atom and the all other surrounding H-atoms act as two coherent sources, separated by a path-length approximately same as the C-H bond length. Thus, the change in the dominant mechanism from pure diffraction in $1a_1$ ionization to interference in $2a_1$ ionization, with the path-length difference being twice as large in the former, one can observe an increase in the period of oscillation for the latte-

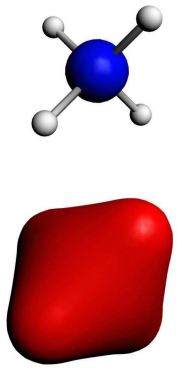

Fig. 5 Equal density contours of the $1a_1$ orbital (upper) and $2a_1$ orbital (lower) in CH_4. The figures are drawn to the same scale. The differences in shape and extent of the two molecular orbitals are readily apparent.

As a matter of fact, all these mechanisms are at work in the $2a_1$ ionization, giving rise to a more irregular oscillation pattern as opposed to the $1a_1$ ionization. This immediately rules out any simple relationship between bond distance and oscillation period, and calls for a more elaborate simulation for the possible reconstruction of the geometrical parameters from the diffraction pattern. Naïvely one assumes each atom as a point source emitter, and this is generally a reasonable assumption in the case of core orbitals, but it is a gross simplification in the case of inner-valence orbitals, as depicted in Figure 5. This does not pose however any additional challenge when a full simulation, taking properly into account the initial orbital as well as the continuum, is employed. The present theoretical model, employing a local DFT potential, is sufficiently computationally efficient that future least-squares simulations appear feasible even for fairly large systems. It remains to be seen if simpler approaches, e.g., modeling the continuum in First Born Approximation[11,28], or the multiple scattering approach[54], may prove viable for more economic alternatives. If on the other side, even more sophisticated theoretical approaches, with fuller treatment of many-body effects, are necessary to retrieve full accuracy, that might significantly limit the scope of the v-ratio diffraction patterns as a tool for structural investigations.

6 Conclusions

In summary, we have carried out detailed experimental and theoretical investigations of the vibrationally resolved $2a_1$ photoionization in CH_4. The photoelectron spectra exhibiting a prominent contribution of the symmetric stretching vibrational mode have been measured over a wide range of photon energies. The possible existence of pre-dissociation as seen in terms of spectral line broadening have been argued by using first-principles theoretical calculations. The observed oscillations in the v-ratios are attributed to the diffraction of photoelectrons in the molecular potential. A sharp low energy feature may be a signature of a so far undetected shape resonance. In contrast to previous observations for $1a_1$ photoionization in CH_4, in the present case the period and shapes of the oscillations are different, and the phases are found to be of opposite sign. This is ascribed to the delocalized nature of the initial orbital, and indicates the need for a full quantum simulation for the reconstruction of the observed profiles, ruling out a simple relationship with the bond distance. In return, information on the composition of the relevant molecular orbital is encoded in the observed oscillations.

7 Acknowledgements

The experiment was performed at the PLÉIADES beamline of the Synchrotron SOLEIL in France (proposal number 99140154 and 99140124). SN thanks E. Antonsson, C. Nicolas for many fruitful discussions, E. Robert for technical assistance, and SOLEIL staff for smooth operation of the machine. EP and FM acknowledge financial support from the European Research Council Advanced Grant No. XCHEM 290853, the MINECO project FIS2013-42002-R, and the European COST Action XLIC CM1204. They also acknowledge allocation of computer time from Mare Nostrum BSC and CCC-UAM.

References

1 H. D. Cohen and U. Fano, *Phys. Rev.*, 1966, **150**, 30.

2 S. K. Semenov, N. A. Cherepkov, M. Matsumoto, T. Hatamoto, X. J. Liu, G. Prümper, T. Tanaka, M. Hoashino, H. Tanaka and F. Gel'mukhanov, *J. Phys. B: At. Mol. Opt. Phys.*, 2006, **39**, L261.

3 X.-J. Liu, N. A. Cherepkov, S. K. Semenov, V. Kimberg, F. Gel'mukhanov, G. Prümper, T. Lischke, T. Tanaka, M. Hoshino and H. Tanaka, *J. Phys. B: At. Mol. Opt. Phys.*, 2006, **39**, 4801.

4 D. Akoury D, K. Kreidi, T. Jahnke, T. Weber, A. Staudte, M. Schöffler, N. Neumann, J. Titze, L. P. Schmidt, A. Czasch, O.

Jagutzki, R. A. Costa Fraga, R. E. Grisenti, R. Díez Muiño, N. A. Cherepkov, S. K. Semenov, P. Ranitovic, C. L. Cocke, T. Osipov, H. Adaniya, J. C. Thompson, M. H. Prior, A. Belkacem, A. L. Landers, H. Schmidt-Böcking and R. Dörner, *Science*, 2007, **318**, 949.

5 K. Kreidi, D. Akoury, T. Jahnke, T. Weber, A. Staudte, M. Schöffler, N. Neumann, J. Titze, L. P. Schmidt, A. Czasch, O. Jagutzki, R. A. Costa Fraga, R. E. Grisenti, M. Smolarski, P. Ranitovic, C. L. Cocke, T. Osipov, H. Adaniya, J. C. Thompson, M. H. Prior, A. Belkacem, A. L. Landers, H. Schmidt-Böcking and R. Dörner, *Phys Rev. Lett.*, 2008, **100**, 133005.

6 B. Zimmermann, D. Rolles, B. Langer, R. Hentges, M. Braune, S. Cvejanovic, O. Geßner, F. Heiser, S. Korica, T. Lischke, A. Reinköster, J. Viefhaus, R. Dörner, V. McKoy and U. Becker, *Nat. Phys.*, 2008, **4**, 649.

7 M. Okunishi, R. Itaya, K. Shimada, G. Prümper, K. Ueda, M. Busuladžić, A. Gazibegović-Busuladžić, D. B. Milošević and W. Becker, *Phys. Rev. Lett.*, 2009, **103**, 043001.

8 S. E. Canton, E. Plésiat, J. D. Bozek, B. S. Rude, P. Decleva and F. Martín, *Proc. Natl. Acad. Sci. USA*, 2011, **108**, 7302.

9 R. Kushawaha, M. Patanen, R. Guillemin, L. Journel, C. Miron, M. Simon, M. N. Piancastelli, C. Skates, and P. Decleva, *Proc. Natl. Acad. Sci. USA*, 2013, **110**, 15201.

10 M. Ilchen, L. Glaser, F. Scholz, P. Walter, S. Deinert, A. Rothkirch, J. Seltmann, J. Viefhaus, P. Decleva, B. Langer, A. Knie, A. Ehresmann, O. M. Al-Dossary, M. Braune, G. Hartmann, A. Meissner, L. C. Tribedi, M. AlKhaldi and U. Becker, *Phys Rev Lett.*, 2014, **112**, 023001.

11 E. Plésiat, L. Argenti, E. Kukk, C. Miron, K. Ueda, P. Decleva and F. Martín, *Phys. Rev. A*, 2012, **85**, 023409.

12 E. Kukk, D. Ayuso, T. D. Thomas, P. Decleva, M. Patanen, L. Argenti, E. Plésiat, A. Palacios, K. Kooser, O. Travnikova, S. Mondal, M. Kimura, K. Sakai, C. Miron, F. Martín and K. Ueda, *Phys. Rev. A*, 2013, **88**, 033412.

13 K. Ueda, C. Miron, E. Plésiat, L. Argenti, M. Patanen, K. Kooser, D. Ayuso, S. Mondal, M. Kimura, K. Sakai, O. Travnikova, A. Palacios, P. Decleva, E. Kukk and F. Martín, *J. Chem. Phys.*, 2013, **139**, 124306.

14 M. Patanen, K. Kooser, L. Argenti, D. Ayuso, M. Kimura, S. Mondal, E. Plésiat, A. Palacios, K. Sakai, O. Travnikova, P. Decleva, E. Kukk, C. Miron, K. Ueda and F. Martín, *J. Phys. B: At. Mol. Opt. Phys.*, 2014, **47**, 124032.

15 D. Ayuso, M. Kimura, K. Kooser, M. Patanen, E. Plésiat, L. Argenti, S. Mondal, O. Travnikova, K. Sakai, A. Palacios, E. Kukk, P. Decleva, K. Ueda, F. Martín and C. Miron, *J. Phys. Chem. A*, 2015, **119**, 6148-6154.

16 S. Chatterjee, D. Misra, A. H. Kelkar, L. C. Tribedi, C. R. Stia, O. A. Fojón and R. D. Rivarola, *J. Phys. B: At. Mol. Opt. Phys.*, 2009, **42**, 065201.

17 L. R. Hargreaves, C. Colyer, M. A. Stevenson, B. Lohmann, O. Al-Hagan, D. H. Madison and C. G. Ning, *Phys. Rev. A*, 2009, **80**, 062704.

18 N. Stolterfoht, B. Sulik, V. Hoffmann, B. Skogvall, J. Y. Chesnel, J. Rangama, F. Frémont, D. Hennecart, A. Cassimi, X. Husson, A. L. Landers, J. A. Tanis, M. E. Galassi and R. D. Rivarola, *Phys. Rev. Lett.*, 2001, **87**, 023201.

19 D. Misra, U. Kadhane, Y. P. Singh, L. C. Tribedi, P. D. Fainstein and P. Richard, *Phys. Rev. Lett.*, 2004, **92**, 153201.

20 J. Y. Chesnel, A. Hajaji, R. O. Barrachina and F. Frémont, *Phys Rev Lett.*, 2007, **98**, 100403.

21 R. P. Crease, *Phys. World*, 2002, **15**, 19.

22 X. J. Liu, Q. Miao, F. Gel'mukhanov, M. Patanen, O. Travnikova, C. Nicolas, H. Ågren, K. Ueda and C. Miron, *Nat. Photon.*, 2015, **9**, 120.

23 F. Martín, *Nat. Photon.*, 2015, **9**, 76.

24 C. Davisson and L. H. Germar, *Phys. Rev.*, 1927, **30**, 705.

25 M. Patanen, O. Travnikova, J. Söderström, P. Decleva, T. D. Thomas, S. Svensson, N. Mårtensson, K. J. Børve, L. J. Sæthre and C. Miron, *Phys. Rev. A*, 2013, **87**, 063420.

26 D. Toffoli and P. Decleva, *Phys. Rev. A*, 2010, **81**, 061201.

27 E. Plésiat, P. Decleva and F. Martín, *Phys. Rev. A*, 2013, **88**, 063409.

28 L. Argenti, T. D. Thomas, E. Plésiat, X. J. Liu, C. Miron, T. Lischke, G. Prümper, K. Sakai, T. Ouchi, R. Püttner, V. Sekushin, T. Tanaka, M. Hoshino, H. Tanaka, P. Decleva, K. Ueda and F. Martín, *New J. Phys.*, 2012, **14**, 033012.

29 J. W. Rabalais, T. Bergmark, L. O. Werme, L. Karlsson and K. Siegbahn, *Phys. Scr.*, 1971, **3**, 13.

30 T. X. Carroll, N. Berrah, J. Bozek, J. Hahne, E. Kukk, L. J. Saethre and T. D. Thomas, *Phys. Rev. A*, 1999, **59**, 3386.

31 U. Hergenhahn, *J. Phys. B: At. Mol. Opt. Phys.*, 2004, **37**, R89.

32 E. Kukk, K. Ueda, U. Hergenhahn, X.-J. Liu, G. Prümper, H. Yoshida, Y. Tamenori, C. Makochekanwa, T. Tanaka, M. Kitajima and H. Tanaka, *Phys. Rev. Lett.*, 2005, **95**, 133001.

33 E. Kukk, T. D. Thomas and K. Ueda, *J. Elec. Spec. Relat. Phenom.*, 2011, **183**, 53.

34 M. Carlsson Göthe, B. Wannberg, L. Karlsson, S. Svensson, P. Baltzer, F. T. Chau and M.-Y. Adam, *J. Chem. Phys.*, 1991, **94**, 2536.

35 E. Kukk, K. Ueda and C. Miron, *J. Elec. Spec. Rel. Phenom.*, 2012, **185**, 278.

36 T. Karlsen and K. J. Børve, *J. Chem. Phys.*, 2000, **112**, 7979.

37 See: http://www.synchrotron-soleil.fr/Recherche/LignesLumiere/PLEIADES.

38 J. Söderström, A. Lindblad, A. N. Grum-Grzhimailo, O. Travnikova, C. Nicolas, S. Svensson and C. Miron, *New J. Phys.*, 2011, **13**, 073014.

39 T. D. Thomas, E. Kukk, K. Ueda, T. Ouchi, K. Sakai, T. X. Carroll, C. Nicolas, O. Travnikova and C. Miron, *Phys. Rev. Lett.*, 2011, **106**, 193009.

40 Q. Miao, O. Travnikova, F. Gel'mukhanov, V. Kimberg, Y. P. Sun, T. D. Thomas, C. Nicolas, M. Patanen and C. Miron, *J. Phys. Chem. Lett.*, 2015, **6**, 1568.

41 Curve fitting macro package SPANCF by E. Kukk [http://www.physics.utu.fi/en/research/material_science/Fitting.html]

42 E. Kukk, J. D. Bozek, G. Snell, W.-T. Cheng and N. Berrah, *Phys. Rev. A*, 2001, **63**, 062702.

43 R. Locht and J. Momigny, *Chem. Phys.*, 1980, **49**, 173.

44 D. Toffoli, M. Stener, G. Fronzoni and P. Decleva, *Chem. Phys.*, 2002, **276**, 25.

45 H. Bachau, E. Cormier, P. Decleva, J. E. Hansen and F. Martín, *Rep. Prog. Phys.*, 2001, **64**, 1815.

46 C. Fonseca-Guerra, J. G. Snijders, G. te Velde and E. J. Baerends, *Theor. Chem. Acc.*, 1998, **99**, 391.

47 C. Angeli, R. Cimiraglia, S. Evangelisti, T. Leininger and J. P. Malrieu, *J. Chem. Phys.*, 2001, **114**, 10252.

48 C. Angeli, R. Cimiraglia and J. P. Malrieu, *J. Chem. Phys.*, 2002, **117**, 9138.

49 MOLPRO, version 2010.1, a package of ab-initio programs, H.-J. Werner, P. J. Knowles, G. Knizia, F. R. Manby, M. Schütz, and others; see http://www.molpro.net.

50 W. Meyer, *J. Chem. Phys.*, 1973, **58**, 1017.

51 L. S. Cederbaum, W. Domcke, J. Schirmer, W. von Niessen, G. H. F. Diercksen and W. P. Kraemer, *J. Chem. Phys.*, 1978, **69**, 1591.

52 K. Ueda, A. Pavlychev, E. Kukk, U. Hergenhahn, H. Yoshida, T. Sunami, F. Tahara, T. Tanaka , M. Kitajima, H. Tanaka, A. De Fanis and Y. Tamenori, *Chem. Phys. Lett.*, 2005, **411**, 33.

53 H. M. Köppe, B. S. Itchkawitz, A. L. D. Kilcoyne, J. Feldhaus, B. Kempgens, A. Kivimäki, M. Neeb and A. M. Bradshaw, *Phys. Rev. A*, 1996, **53**, 4120.

54 J. J. Rehr and R. C. Albers, *Rev. Mod. Phys.*, 2000, **72**, 621.